Polymer Chemistry

Accepted Manuscript

ROYAL SOCIETY OF CHEMISTRY

www.rsc.org/polymers

Hybrid porous polymers derived from cubic octavinylsilsequioxane and planar halogenated benzene monomers exhibit high thermal stability, tunable porosities and potential applications in carbon dioxide storage.

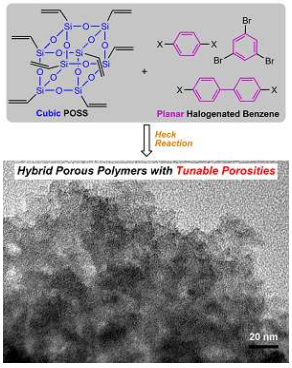

Cite this: DOI: 10.1039/c0xx00000x

www.rsc.org/xxxxxx

ARTICLE TYPE

Constructing Hybrid Porous Polymers from Cubic Octavinylsilsequioxane and Planar Halogenated Benzene†

Dengxu Wang[a,b], Wenyan Yang[b], Shengyu Feng*[a,b] and Hongzhi Liu*[b]

Received (in XXX, XXX) Xth XXXXXXXXX 20XX, Accepted Xth XXXXXXXXX 20XX

DOI: 10.1039/b000000x

Heck coupling of cubic octavinylsilsequioxane (OVS) with planar di-/tri- halogenated benzene (**1**–**5**) results in a series of inorganic–organic hybrid porous polymers (HPPs). These materials show high thermal stability and tunable porosities with Brunauer–Emmer–Teller surface areas ranging from 479 m^2 g^{-1} to 805 m^2 g^{-1}, and with total pore volume ranging from 0.33 cm^3 g^{-1} to 0.59 cm^3 g^{-1}. Porosity comparison reveals that monomer species and reaction condition strongly affect surface area, pore volume and microporosity. For the monomer species, monomers with high reactivity, long strut length and more connectable sites are beneficial to enhance the surface area and pore volume. For the reaction condition, the condition which can result in high levels of coupling degrees and the choice of *N*,*N*-dimethylformamide (DMF) as the solvent can also enhance the porosity. However, long monomer strut length may also lead to the lower surface area and pore volume. DMF tends to increase the level of microporosity and increasing connectable sites may afford more mesopores. These results suggest that these comprehensive factors should be carefully considered when preparing new porous polymers with controllable porosity. In the application, HPP-3 possesses a moderate carbon dioxide uptake of 1.38 mmol g^{-1} (6.1 wt%) at 273 K and 0.68 mmol g^{-1} (2.99 wt%) at 298 K when measured up to 1 bar. HPP-3 shows a high binding ability with CO_2 with an isosteric heat of 35 kJ mol^{-1} at low coverage, making these materials become promising candidates for storing and capturing CO_2.

Introduction

Porous materials have rapidly developed for several years due to their widely potential applications in gas storage, separation, catalysis and electronics.[1-8] Recently, covalently linked porous polymers have attracted specific interests of scientists since they possess intrinsic properties of large specific surface areas, high thermal and chemical stability, and low skeletal density.[9-13] Compared with other porous materials such as zeolites and metal-organic frameworks (MOFs),[3-5] porous polymers have an advantage in that their structures and properties could be easily modified through rational chemical design because of the diversified selection of monomers and chemical synthetic routes.[9,10] These factors provide a wealth of opportunities to control the porous structures as well as framework and surface functionalities, which are also the major goal in this area because the porosity and functionality play crucial roles in their applications.

To prepare porous polymers with stable pores, it is typically necessary to use rigid building units that can prevent the networks from collapsing and hence filling space in an efficient manner. Rigidity often results from the aromatic monomers, either directly linked together or linked by other rigid groups.[10] From the standpoint of monomer structures, monomers with diversified geometries such as linear,[14] planar,[15] tetrahedral,[16] and octahedral[17] geometries can provide suitable rigidity to afford the porosity. Linking the monomers with different geometries together can combine their advantages and the porosity and functionality of the resulting polymers could be easily tuned.[18-20] For example, the surface area and pore dimension in microporous poly(aryleneethynylene) (PAE) networks can be controlled by monomer structure, i.e., monomer strut length; Brunauer-Emmett-Teller (BET) surface areas (S_{BET}) ranged from 512 m^2 g^{-1} to 1018 m^2 g^{-1}.[18]

Polyhedral oligomeric silsesquioxanes (POSS, typically cubic $R_8Si_8O_{12}$) are an ideal class of building blocks to construct porous polymers because they are rigid, highly functional and exceptionally robust with respect to heat and water; the presence of inorganic–organic hybrid POSS units provides high thermal stability and opportunities for further functionalization by post-synthetic methods.[21,22] POSS-based porous polymers can be prepared by using three strategies: (i) self-crosslinking of functional POSS;[23,24] (ii) crosslinking of different functional POSS[25,26] and (iii) crosslinking of functional POSS with other rigid monomers.[27,28] Compared with the first two, porosity and functionality is easier to tune using the third strategy. For example, Sonagashira cross-coupling of bromophenylethenyl-terminated POSS with di/triethynyl compounds resulted in microporous networks with S_{BET} ranging from 850 m^2 g^{-1} to 1040 m^2 g^{-1} depending on the length and the connectable sites of the ethynyl compounds.[27] Simultaneously using

octavinylsilsesquioxane (OVS) and tetrahedral silicon-centered precursors as building blocks, the resulting networks exhibited tunable porosity from almost no porosity to high porosity with S_{BET} of up to 875 $m^2 g^{-1}$ as well as blue luminescence.[28]

Cubic OVS is the most commonly used monomer among various POSS derivatives because of its low-cost and easy accessibility,[22] while planar halogenated benzene are easily accessible compounds among aromatic monomers. In the present study, we utilized these two kinds of monomers, i.e., OVS and di/tri- halogenated benzene (**1**–**5**) to construct novel inorganic-organic hybrid porous polymers (HPPs) by Heck coupling (see Scheme 1). Meanwhile, for a selected synthesis methodology, many parameters such as chemical synthesis routes, monomer species, molecular weight, and reaction condition influence the porous structure and targeted site-specific functionalities in the final products.[9,29-32] In the present study, the factors including monomer species and reaction condition on the porosity of the resulting polymers were investigated. Finally, their applications in carbon dioxide (CO_2) storage were also explored.

Experimental Section

Materials

Unless otherwise noted, all reagents were obtained from commercial suppliers and used without further purification. OVS was synthesized by the previous report.[33] Tetrahydrofuran (THF) was dried by distillation over sodium metal prior to use. *N*,*N*-dimethylformamide (DMF) was first dried over CaH_2 at 80ºC for 12 h, distilled under vacuum pressure and stored with 4 Á molecule sieves prior to use. Triethylamine (Et_3N) was dried over CaH_2 and used freshly.

Characterization

Fourier transform infrared (FTIR) spectra of the products were recorded on a Bruker Tensor27 spectrophotometer. Solid-state ^{13}C cross-polarization/magic-angle-spinning (CP/MAS) NMR and ^{29}Si MAS NMR spectra were performed on Bruker AVANCE-500 NMR Spectrometer operating at a magnetic field strength of 9.4 T. The resonance frequencies at this field strength were 125 and 99 MHz for ^{13}C NMR and ^{29}Si NMR, respectively. A chemagnetics 5 mm triple- resonance MAS probe was used to acquire ^{13}C and ^{29}Si NMR spectra. ^{29}Si MAS NMR spectra with high power proton decoupling were recorded using a $\pi/2$ pulse length of 5 μs, a recycle delay of 120 s and a spinning rate of 5 kHz. Elemental analyses were conducted using an Elementar vario EL III elemental analyzer and Oxford INCA X-sight energy dispersive X-ray spectrometry.

Field-emission scanning electron microscopy (FE-SEM) experiments were performed by using HITACHI S4800 Spectrometer. The high-resolution transmission electron microscopy (HR-TEM) experiments were performed by using a JEM 2100 electron microscope (JEOL, Japan) with an acceleration voltage of 200 kV.

Thermogravimetric analyses were performed with a MettlerToledo SDTA-854 TGA system in nitrogen at a heating rate of 10 ºC min^{-1} to 800ºC. Powder X-ray diffraction (PXRD) were performed using a Riguku D/MAX 2550 diffractometer under Cu-Kα radiation, 40 kV, 200 mA with a scanning rate of 10 ° min^{-1} (2θ).

Nitrogen sorption isotherm measurements were performed on a Micro Meritics surface area and pore size analyzer. Before measurement, samples were degassed at 100ºC for least 12 h. A sample of ca. 100 mg and a UHP-grade nitrogen (99.999%) gas source were used in the nitrogen sorption measurements at 77 K and collected on a Quantachrome Quadrasorb apparatus. BET surface areas were determined over a P/P_0 range from 0.01 to 0.20. Nonlocal density functional theory (NL-DFT) pore size distributions were determined using the carbon/slit-cylindrical pore mode of the Quadrawin software. Carbon dioxide (CO_2) adsorption isotherms at 298 K and 273 K were measured on a Micrometrics ASAP 2020. Prior to the measurements, the samples were degassed at 150 °C for at least 15 h.

Synthesis of hybrid porous polymers, HPP-1 to HPP-3

HPP-1a. In an oven-dried flask, OVS (632 mg, 1 mmol), palladium acetate (90 mg, 0.4 mmol) and triphenylphosphine (210 mg, 0.8 mmol) were added with THF/Et_3N (45 mL/15 mL) under argon. The mixture was stirred and bubbled by argon under stirring for 0.5 h at room temperature and 1,4-diiodobenzene (**1**) (1.32 g, 4 mmol) was added. The reaction mixture was then heated at 80ºC for 48 h. After cooling to room temperature, the mixture was filtered and washed with THF, chloroform, water, methanol and acetone to remove any amine salts, unconsumed monomers and catalyst residues. Further purification of the sample was carried out by extraction with THF for 24 h and methanol for 24 h. The product was recovered by filtration, and dried under reduced pressure at 70 ºC for 48 h. HPP-1a was obtained as a red-brown solid (1.05 g). Yield: 113%. The yield was calculated based on hypothetical 100% polycondensation and no destruction of POSS cages. Elemental analysis calc. (wt.%) for $C_{40}H_{32}Si_8O_{12}$: C 51.69, H 3.47; Found C 49.22, H 4.15, N 0.042. Coupling degree: 96.70%.

HPP-1b. OVS (632 mg, 1 mmol), palladium acetate (90 mg, 0.4 mmol), and tris(2-methylphenyl)phosphine (193 mg, 0.94 mmol) were dissolved in a DMF/Et_3N solution (45 mL/15 mL) under argon. The mixture was stirred and bubbled by argon under stirring for 0.5 h at room temperature, after which 1,4-diiodobenzene (**1**) (1.32 g, 4 mmol) was added. The resulting solution was then heated at 100 °C for 48 h and cooled to room temperature. The purification of the crude product was similar to that of HPP-1a. HPP-1b was obtained as a red-brown solid (1.02 g). Yield: 109%. Elemental analysis calc. (wt.%) for $C_{40}H_{32}Si_8O_{12}$: C 51.69, H 3.47; Found C 51.02, H 4.36, N 0.055. Coupling degree: 99.96%.

HPP-1c. The synthesis procedure and post-treatment of HPP-1c were similar to those of HPP-1b except that 1,4-diiodobenzene (**1**) (1.32 g, 4 mmol) was replaced by 1,4-dibromobenzene (**2**) (1.25 g, 4 mmol). HPP-1c was obtained as a gray-green solid (1.05 g). Yield: 113%. Elemental analysis calc. (wt.%) for $C_{40}H_{32}Si_8O_{12}$: C 51.69, H 3.47; Found C 49.05, H 4.29, N 0.11. Coupling degree: 97.80%.

HPP-2a. The synthetic procedure and post-treatment of HPP-2a were similar to those of HPP-1a except that 1,4-diiodobenzene (**1**) (1.32 g, 4 mmol) was replaced by 1,4-diiodobiphenyl (**3**) (1.62 g, 4 mmol). HPP-2a was obtained as a red-brown solid (1.23 g). Yield: 100%. Elemental analysis calc. (wt.%) for $C_{64}H_{48}Si_8O_{12}$: C 62.30, H 3.92; Found C 58.85, H 4.50, N 0.15. Coupling degree: 97.66%.

HPP-2b. The synthetic procedure and post-treatment of HPP-2b were similar to those of HPP-1b except that 1,4-diiodobenzene (**1**) (1.32 g, 4 mmol) was replaced by 1,4-diiodobiphenyl (**3**) (1.62 g, 4 mmol). HPP-2b was obtained as a gray-green solid (1.26 g). Yield: 102%. Elemental analysis calc. (wt.%) for $C_{64}H_{48}Si_8O_{12}$: C 62.30, H 3.92; Found C 59.52, H 4.58, N 0.096. Coupling degree: 99.96%.

HPP-2c. The synthetic procedure and post-treatment of HPP-2c were similar to those of HPP-1c except that 1,4-dibromobenzene (**2**) (1.25 g, 4 mmol) was replaced by 1,4-dibromobiphenyl (**4**) (1.62 g, 4 mmol). HPP-2c was obtained as a gray-green solid (1.27 g). Yield: 103%. Elemental analysis calc. (wt.%) for $C_{64}H_{48}Si_8O_{12}$: C 62.30, H 3.92; Found C 59.04, H 4.60, N 0.13. Coupling degree: 99.57%.

HPP-3. The synthetic procedure and post-treatment of HPP-3 were similar to those of HPP-1c except that 1,4-dibromobenzene (**2**) (1.25 g, 4 mmol) was replaced by 1,3,5-tribromobenzene (**5**) (0.91 g, 2.67 mmol). HPP-3 was obtained as a blackish green solid (1.25 g). Yield: 101%. Elemental analysis calc. (wt.%) for $C_{32}H_{24}Si_8O_{12}$: C 36.39, H 3.49; Found C 34.53, H 4.06, N 0.16. Coupling degree: 98.27%.

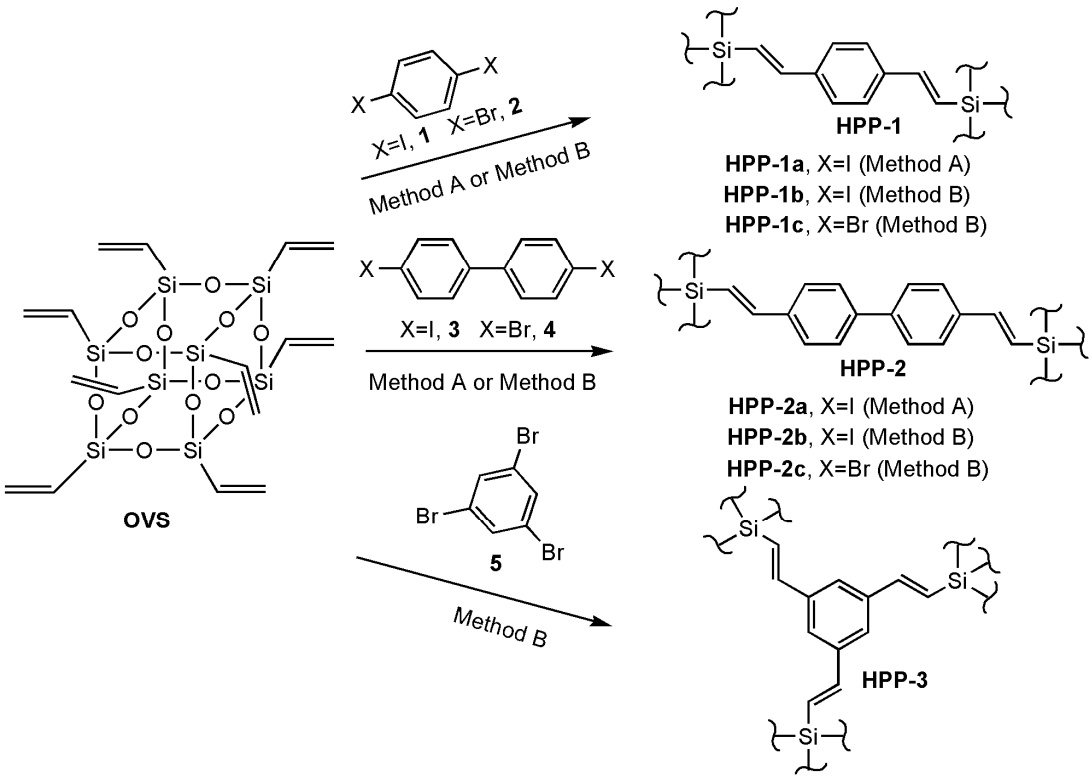

Scheme 1 The synthetic routes of hybrid porous polymers, HPP-1 to HPP-3. Method A: $Pd(OAc)_2/PPh_3$, THF/Et_3N, 80ºC, 48h; Method B: $Pd(OAc)_2/P(o\text{-}CH_3Ph)_3$, DMF/Et_3N, 80ºC, 48h.

Results and Discussion

We have demonstrated recently that Heck reaction can be used to prepare hybrid porous polymers.[25,28] Similar to other polycondensation techniques such as Sonogashira-Hagihara coupling[29,34] and Yamamoto coupling[16,35,36] for generating porous networks, a number of factors[37] including monomer reactivity (i.e., the selection of iodinated or brominated monomers), monomer structure, catalyst, solvent and temperature may influence the porosity of the resulting materials via Heck reaction.

In the present study, we utilized OVS and commercially available halogenated benzene, including 1,4-diiodobenzene (**1**), 1,4-dibromobenzene (**2**), 4,4'-diiodo-biphenyl (**3**), 4,4'-dibromobi-phenyl (**4**), and 1,3,5-tribromobenzene (**5**) as monomers, and a series of novel porous polymers, HPP-1 to HPP-3, were obtained (Scheme 1). To investigate the factors on the porosities of these polymers, these reactions were carried out in two conditions: One was at 80ºC in THF using $Pd(OAc)_2/PPh_3$ as the catalyst for 48 h (method A); Another was at 100°C in DMF using $Pd(OAc)_2/P(o\text{-}CH_3Ph)_3$ as the catalyst for 48 h (method B). Obviously, method B endowed the reactions much higher reaction activity than method A. For iodinated monomers (**1** and **3**), the resulting polymers, HPP-1a and HPP-1b from **1**, and HPP-2a and HPP-2b from **3**, were synthesized using methods A and B, respectively. For brominated monomers (**2**, **4** and **5**), the resulting polymers, HPP-1c, HPP-2c and HPP-3, were prepared using method B. The choice of the reaction condition was attributed to the lower reactivity of brominated monomers than iodinated monomers. After the reactions, the crude products were recovered by filtration, washed and extracted with several solvents, and dried under vacuum at 70 ºC for 48 h to yield the materials. Similar to our recent reports,[25,28] the relatively large difference between the calculated and theoretical contents of C, H and N by elemental analysis could be ascribed to a small number of remaining end groups and the residual amine salts, solvents or catalysts in the final products. This speculation can be proven by the very small amounts of N and Br contents found by elemental

analysis and energy dispersive X-ray spectrometry (EDS) (Fig. S1).

The coupling degrees of these polymers were all > 97% as calculated by elemental analysis of the C, O, Si, X (X = Br or I) contents based on EDS results (Fig. S1). The coupling degrees of HPP-1a and HPP-2a from iodinated monomers using method A were 96.7% and 97.6%, which were much higher than those from iodinated octaphenylsilsequioxane (OPS) and OVS in our recent report (64% and 62%).[25] This difference can be attributed to the different molecular geometries of planar monomers and octahedral POSS-based monomers. In the previous report,[25] the networks were linked by two octahedral monomers, namely, iodinated OPS and OVS. To completely react all the reactive groups and form the connections groups, –CH=CH–Ph, the geometry of the monomers should arrange in a long-range ordering. However, the ordering formation is very difficult and the linking is generally random because of the large molecular dimensions and steric hindrance of POSS-based monomers even if they are rigid. Thus many reactive groups were residual in the interior and terminal regions of the final products. However, for the planar monomers (**1** and **3**), their molecular dimensions were small and they were more flexible than octahedral monomers when linked with these monomers. Thus higher coupling degrees were obtained in HPP-1a and HPP-2a. The coupling degrees of HPP-1b and HPP-2b from method B were > 99.9% and higher than method A, which was obviously due to higher reaction activity in method B. It is noted that the polymers from brominated monomers in method B also exhibited high coupling degrees (> 97%). These results revealed that Heck coupling reaction could be applied as an efficient methodology to construct porous polymers.

The structures of the resulting polymers were characterized by FTIR, solid-state ^{13}C CP/MAS NMR and ^{29}Si MAS NMR spectroscopy. HPP-1a, HPP-2a and HPP-3 were selected as representative samples. Fig. 1 shows the FTIR spectra of OVS and the polymers. The C=C stretching vibration peaks for OVS were observed at 1606 cm^{-1}. Stronger and more aromatic C=C stretching vibration peaks (e.g., HPP-2a: 1440, 1490, and 1569 cm^{-1}) appeared for the polymers because of the introduction of phenyl rings. Compared with the Si-O-Si stretching vibration for OVS at ca. 1110 cm^{-1}, those for the porous networks became broader, indicating the presence of cross-linking networks.[24-28,38]

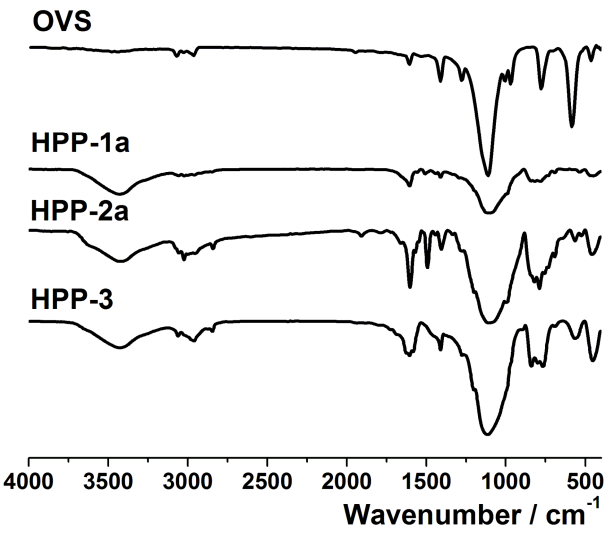

Fig. 1 FTIR spectra of OVS, HPP-1a, HPP-2a and HPP-3.

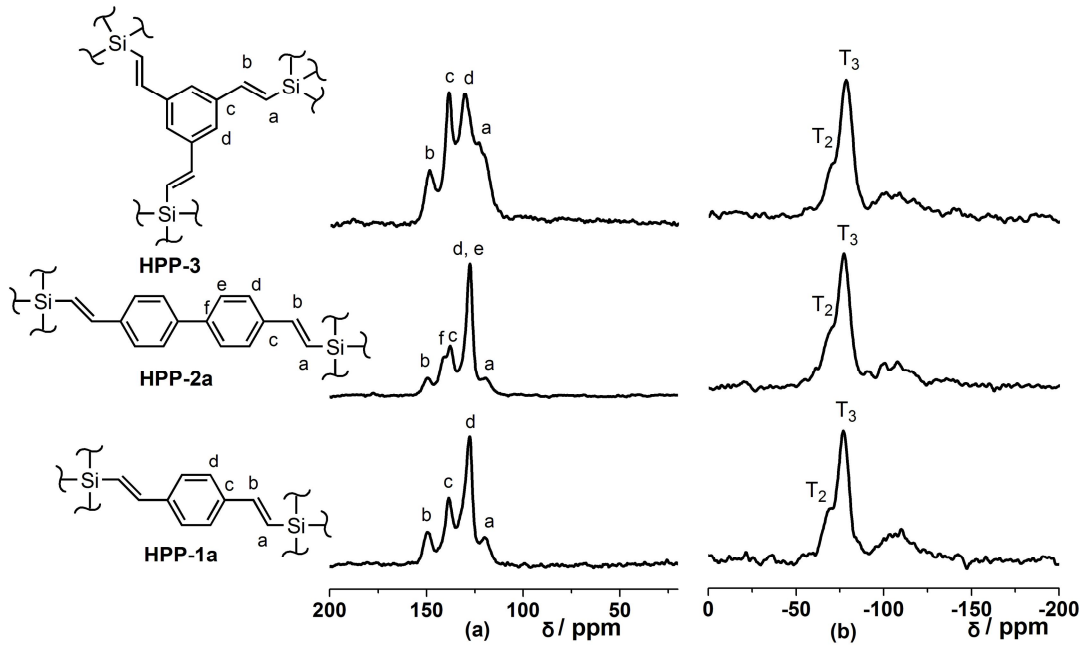

Fig. 2 Solid-state ^{13}C CP/MAS NMR (a) and ^{29}Si MAS NMR (b) spectra of HPP-1a, HPP-2a and HPP-3.

Fig. 2 shows the solid ^{13}C CP/MAS NMR and ^{29}Si MAS NMR spectra of HPP-1a, HPP-2a and HPP-3. The signals arising from ethenylene carbon atoms (Si*C*H=CH and SiCH=*C*H) were observed at ca. 119 ppm and 149 ppm (Fig. 2a), which confirms the formation of internal double bonds between the vinyl and halogenated phenyl units.[24,25,27,28] The signals from 120 ppm to 140 ppm can be attributed to sp^2 phenylene carbon atom derived from the bridging phenyl units. The solid-state ^{29}Si NMR spectra

exhibited two main signals at ca. -70 ppm and -78 ppm (Fig. 2b), which can be assigned to T_2 and T_3 units (T_n: $CSi(OSi)_n(OH)_{3-n}$). This finding confirms the presence of POSS moieties and indicates that partial POSS cages collapsed during synthesis, consistent with POSS-based porous polymers previously studied.[24,25,27,28] In addition, the appearance of broad peaks centered at ca. -105 ppm may be ascribed to Q_n ($Si(OSi)_n(OH)_{4-n}$) species[39] and suggests that Si-C bonds have been partially cleaved. Similar to our recent reports,[25,28] such destructions can be caused by two reasons: (i) First, triethylamine must be employed to absorb the generated HBr in Heck reaction and the basic environment could cleave the siloxane and Si-C bonds; and (ii) second, the partial destruction of POSS cages may occur when the cubic POSS cages were linked by rigid connections to form cross-linking networks. However, most of POSS cages remained intact in the networks.

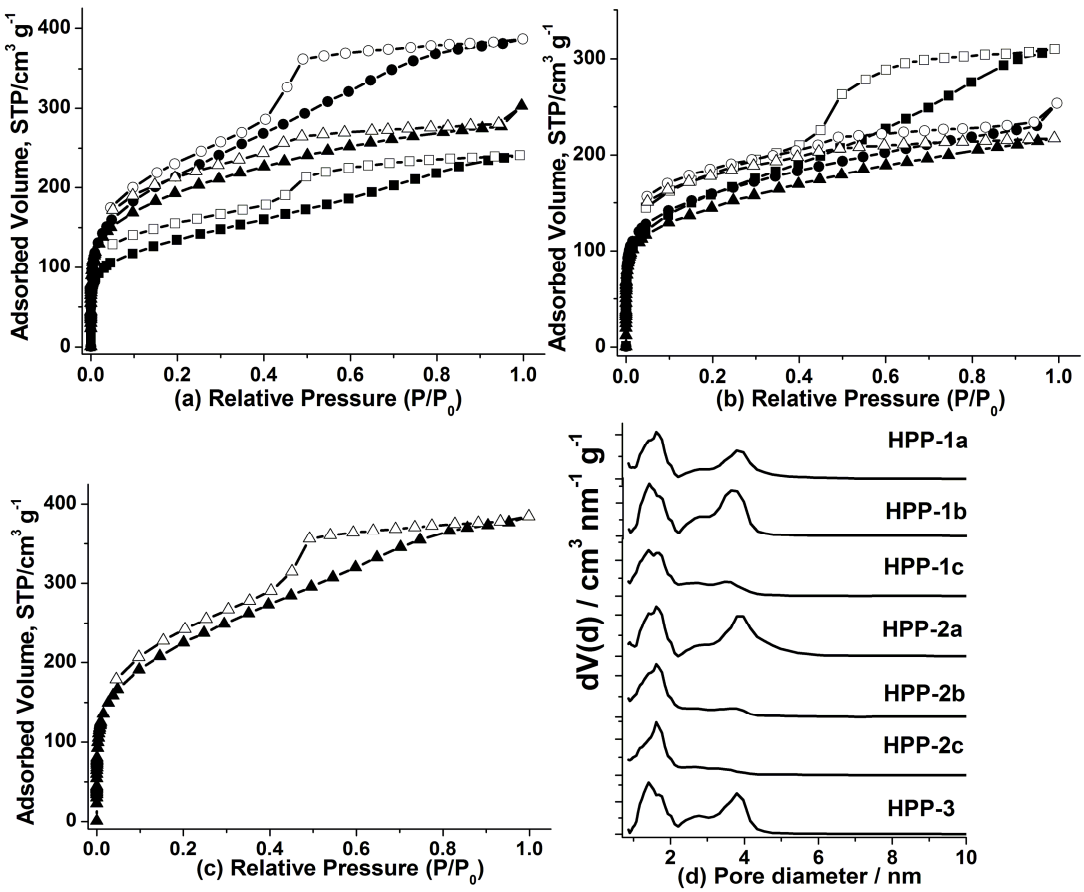

Fig. 3 Nitrogen adsorption (closed symbols) and desorption (open symbols) isotherms for HPP-1 (a), HPP-2 (b) and HPP-3 (c) (■□: HPP-1a and HPP-2a; ●○: HPP-1b and HPP-2b; ▲△: HPP-1c, HPP-2c and HPP-3); (d) pore size distribution curves of HPP-1 to HPP-3.

Table 1. Porosity data of HPP-1, HPP-2 and HPP-3

HPPs	S_{BET}[a]/ $m^2\ g^{-1}$	S_{micro}[b]/ $m^2\ g^{-1}$	V_{total}[c]/ $cm^3\ g^{-1}$	V_{micro}[d]/ $cm^3\ g^{-1}$	V_{micro}/V_{total}
HPP-1a	479	182	0.37	0.091	0.24
HPP-1b	776	238	0.59	0.11	0.19
HPP-1c	690	391	0.46	0.18	0.39
HPP-2a	569	203	0.47	0.10	0.21
HPP-2b	566	358	0.38	0.17	0.44
HPP-2c	513	318	0.33	0.15	0.45
HPP-3	805	307	0.59	0.15	0.25

[a] Surface area calculated from N_2 adsorption isotherm using the BET method; [b] Microporous surface area calculated from N_2 adsorption isotherm using *t*-plot method; [c] Total pore volume calculated at P/P_0 = 0.99; [d] Micropore volume derived using the *t*-plot method based on the Halsey thickness equation.

The porosities in these polymers were investigated by nitrogen sorption isotherm measurements at 77 K from which S_{BET}, microporous surface area (S_{micro}), total pore volume (V_{total}), and micropore volume (V_{micro}) were calculated. Fig. 3a-c show the N_2 isotherms for polymers HPP-1 to HPP-3 and Table 1 summarizes the porosity data of each polymer. The nitrogen isotherms for HPP-1c, HPP-2b and HPP-2c exhibited type I isotherms, while other polymers gave rise to type I N_2 isotherms with some type IV isotherm characteristics at higher relative pressure according to IUPAC classifications. All of the N_2 isotherms for the polymers exhibited a sharp uptake at relative low pressure and gradually increasing uptake at higher relative pressure with hysteresis to a degree, suggesting the presence of micropore and mesopore within the networks. These polymers exhibited tunable porosities with S_{BET} ranging from 479 $m^2\ g^{-1}$ (HPP-1a) to 805 $m^2\ g^{-1}$ (HPP-3) and V_{total} ranging from 0.33 $cm^3\ g^{-1}$ (HPP-2c) to 0.59 $cm^3\ g^{-1}$ (HPP-1b and HPP-3) by altering the monomer species and reaction condition. The ratios of V_{micro}/V_{total}, which indicates how microporous a material is (i.e., how much the pore volume

arises from micropores rather than mesopores or interparticular porosity), ranged from 0.19 (HPP-1b) to 0.45 (HPP-2c) in these polymers. The pore size distributions (PSDs) were evaluated by nonlocal density functional theory (NL-DFT). These polymers exhibited similar PSD curves with two main peaks: a narrow micropore distribution centered at ~1.5 nm and a relatively broad mesoprore distribution centered at ~3.7 nm (Fig. 3d). The results agreed with the shape of the N_2 isotherms and suggested that the structures all featured micropores and mesopores.

Fig. 4 shows the comparisons of S_{BET}, V_{total} and V_{micro}/V_{total} for the polymers. Based on the porosity data, it is clear that the porosity is evidently affected by the monomer species and reaction condition. For the series of polymers HPP-1, S_{BET} and V_{total} for HPP-1a derived from OVS and **1** under method A were 479 m^2 g^{-1} and 0.37 cm^3 g^{-1}, respectively. When method A was replaced by method B, S_{BET} and V_{total} were evidently enhanced to 776 m^2 g^{-1} and 0.59 cm^3 g^{-1}, respectively, in the resulting polymer HPP-1b. The occurrence of this phenomenon can be attributed to the higher coupling efficiencies and the choice of reaction solvent. It has demonstrated that the efficiencies of the bonding chemistries had a strong influence on the surface area and pore volume of the resulting porous networks.[34] Obviously method B endowed the reaction higher activity than method A, thereby resulting in higher coupling degree and reaction rate. The coupling degree of HPP-1b (99.96%) was higher than that of HPP-1a (96.70%). Higher reaction rate for HPP-1b than HPP-1a could be verified by the initial formation time of the cross-linking products, which were observed visually at ca. 2 h and 20 min for HPP-1a and HPP-1b, respectively. The surface area and pore volume were also strongly affected by the choice of reaction solvent. Cooper et al. proved that networks formed in DMF tended to exhibit the highest surface areas and the highest levels of microporosity among a series of reaction solvents, including toluene, THF, dioxane and DMF.[29] In the present study, the selection of DMF for HPP-1b rather than THF for HPP-1a led to higher surface area.

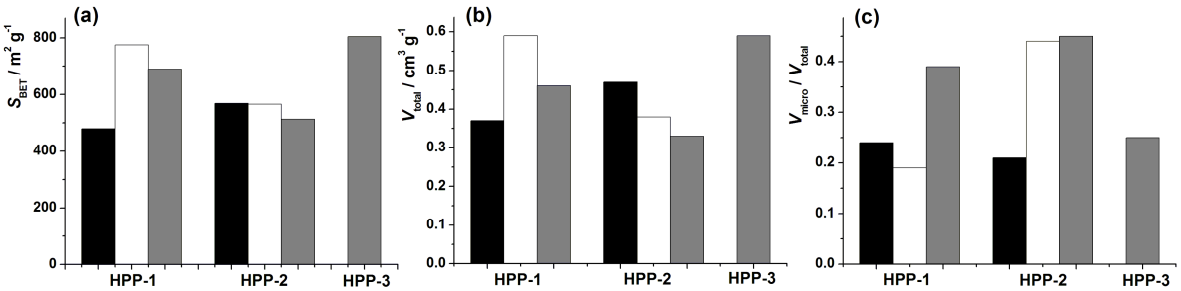

Fig. 4 BET surface area (S_{BET}) (a), total pore volume (V_{total}) (b) and micropore volume over total pore volume (V_{micro}/V_{total}) (c) for HPP-1 to HPP-3. Black: HPP-1a and HPP-2a; Blank: HPP-1b and HPP-2b; Gray: HPP-1c, HPP-2c and HPP-3.

When iodinated monomer (**1**) was replaced by brominated monomer (**2**) under method B, the resulting polymer HPP-1c showed lower S_{BET} and V_{total} than HPP-1b, which can be attributed to the lower reactivity of brominated monomers than iodinated monomers. However, S_{BET} and V_{total} of HPP-1c were higher than those of HPP-1a, indicating that the reaction condition might play a superior effect on the porosity. By contrast, the coupling degree for HPP-1c was 97.80% and the initial formation time of cross-linking products was observed visually at ca. 5 h. Among HPP-1a, HPP-1b and HPP-1c, HPP-1c exhibited the highest levels of microporosity (Fig. 4c). This result was induced by the utilization of DMF as described above,[29] although a slight decrease occurred in HPP-1b compared with HPP-1a.

However, the porosity trend for the series of polymers HPP-2 in terms of the monomer species and reaction condition was different from HPP-1. HPP-2 showed similar surface area with S_{BET} ranging from 510 m^2 g^{-1} to 570 m^2 g^{-1}, as well as a relatively slight difference of V_{total} ranging from 0.33 cm^3 g^{-1} to 0.47 cm^3 g^{-1}. This difference may be affected by the different strut length of the resulting linker between the connecting nodes except the coupling efficiencies and the choice of reaction solvent. The connecting linker of HPP-2, –CH=CH–Ph–Ph–CH=CH–, was longer than that of HPP-1, –CH=CH–Ph–CH=CH–. Previous reports have demonstrated that the porosity can be fine tuned by the monomer structure, particularly by the monomer strut length.[18,28] In a certain range, longer linkers can increase the surface area and pore volume. For example, S_{BET} and V_{total} for HPP-1a were much higher than the porous polymer with the linkers –CH=CH–Ph– synthesized from iodinated OPS and OVS (S_{BET}: 382 m^2 g^{-1}; V_{total}: 0.23 cm^3 g^{-1}) likewise using method A.[25] However, longer linkers possess increased degree of conformational freedom, which results in greater intermolecular and intramolecular intercalation as well as more efficient space filling in the structures; the results lead to lower micropore volumes and surface areas.[18] This effect can be proven by the fact that S_{BET} and V_{total} for HPP-2b and HPP-2c were lower than those for HPP-1b and HPP-1c. Therefore, the multi-factor effect resulted in the porosity trend for HPP-2. Additionally, higher levels of microporosity for HPP-2b and HPP-2c, than HPP-2a also proved the effect of DMF, in which micropores are easily obtained in comparison to other solvents as described above.[29]

When monomers **1**–**4** were replaced by monomer **5**, the resulting polymer HPP-3 exhibited higher surface area with S_{BET} of 805 m^2 g^{-1} and pore volume with V_{total} of 0.59 cm^3 g^{-1} than both HPP-1 and HPP-2 except that HPP-1b and HPP-3 possessed the same V_{total}. This result suggests that another important effect, i.e., the connectable sites of monomers should be also considered when constructing porous polymers because more connectable sites means higher cross-linking density, which can be expected to lead to less interpenetration and thus afford a greater degree of permanent pore volume.[34] Evidently, the network HPP-3 possessed higher cross-linking density than HPP-1 and HPP-2. However, increasing cross-linking density may afford more mesopres. HPP-3 featured more mesopores and a much lower level of microporosity than HPP-1c and HPP-2c; these polymers

were derived from the same species of monomers, i.e., brominated monomers under the same reaction condition.

On the basis of these results, the porosity of porous polymers was affected by multiple factors such as monomer species, monomer structure, catalyst, and solvent ─ that is, it is difficult to increase/decrease the porosity by merely altering one or two factors. However, these results could give the researchers some information on the design and synthesis of porous polymers with tunable/controllable surface area, pore volume and microporosity. To increase the surface areas and pore volumes, the factors including long monomer strut length, high monomer reactivity, more connectable sites of monomers, high levels of coupling degrees and the choice of DMF should be preferentially considered. In addition, long monomer strut length may also lead to lower pore volumes and surface areas because of greater interpenetration and more efficient space filling in the structures. DMF might be a positive factor that can increase the level of microporosity, whereas increasing connectable sites may afford more mesopores. Thus comprehensive factors should be carefully considered to control the porosity of porous polymers.

To evaluate the thermal stability of these polymers, thermogravimetric analysis (TGA) was performed under N_2 at 10 °C min^{-1}. Consistent with our recent report,[40] the initial decomposition of OVS is ascribed to cleavage of the peripheral vinyl groups. The sharp mass loss at ca. 300°C indicates the overlapping destructions of POSS cage and vinyl groups (Fig. S5). The low residual of OVS is attributed to volatilization, which is the evaporation or sublimation. This phenomenon is similar to the thermal degradation behaviors of other POSS derivatives such as hydrogen POSS and some alkyl-substituted POSS (e.g. methyl, ethyl and isobutyl).[41] All the polymers were very stable up to ca. 450 °C (decomposition temperature at 5% mass loss) and were significantly more stable than OVS because of the highly cross-linking networks (Fig. S5). Initial mass loss can be attributed to the destruction of organic moieties, i.e., ethenylene phenyl groups. Then the decomposition appeared at ~520°C, which may be derived from some mass loss from siloxane spacers. Moreover, the thermal stabilities of the polymers were comparable or more stable than other porous POSS-based and organic polymers.[23-29,42,43]

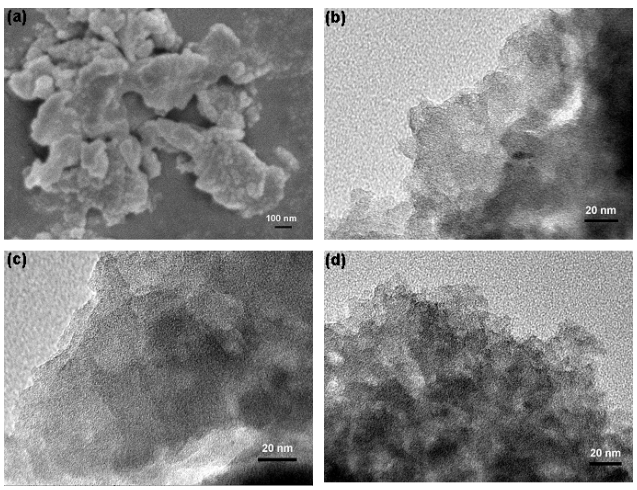

Fig. 5 (a) FE-SEM image of HPP-1a; HR-TEM images of (b) HPP-1a, (c) HPP-2a and (d) HPP-3.

As expected, the polymers were amorphous and powder X-ray diffraction patterns revealed no long-range crystallographic order (Fig. S6). The broad diffraction peaks at ~22° 2θ were associated with the Si-O-Si linkages.[23-28] Scanning electron microscopy (SEM) of the samples showed porous networks formed by inter-linking of irregular shapes with a wide range of size distribution from 100 nm to tens of micrometers (Fig. 5a and Fig. S7). The texture and ordering of these materials were evaluated by high-resolution transmission microscopy (HR-TEM). The TEM images revealed that the polymers showed the characteristics of porous materials with a relatively uniform diameter, but no evidence of long-range ordering was observed (Fig. 5b-d, HPP-1a, HPP-2a and HPP-3 as representative samples). It is noted that the samples were very stable under the electron beam.

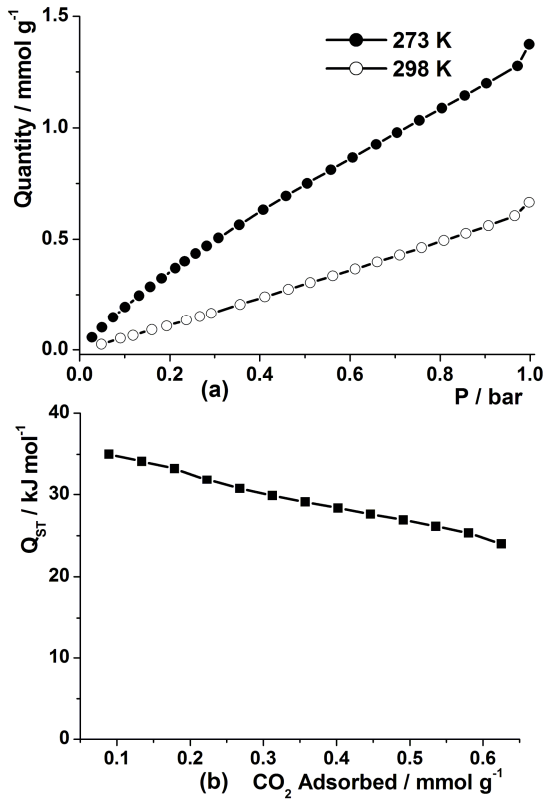

Fig. 6 (a) Carbon dioxide adsorption isotherms at 273 K and 298 K; (b) Isosteric heat of carbon dioxide adsorption.

In recent years, the capture and storage of CO_2 have become an important topic because CO_2 is thought to be a major contributor to global warming.[44-46] A typical kind of solid adsorbents for capturing CO_2 is porous polymers.[10] Therefore, we carried out CO_2 adsorption experiments at 273 K and 298 K to evaluate the potential application of these porous polymers and HPP-3 was selected as an example. The uptakes of HPP-3 were found to be 1.38 mmol g^{-1} (6.1 wt%) at 273 K and 0.68 mmol g^{-1} (2.99 wt%) at 298 K, which were measured up to 1 bar (Fig. 6a). This capacity was comparable to the corresponding values of some MOFs materials,[47] COFs materials[48] and porous polymers[49] with a level of surface areas. The isosteric heat of adsorption, which was calculated from the CO_2 isotherms collected at 298 K and 273 K employing the Clausius-Clapeyron equation, was 35 kJ mol^{-1} at low coverage, and it gradually dropped at higher

coverage (Fig. 6b). This value was higher than that of some porous polymers.[50] This result demonstrated that HPP-3 possessed a high binding ability with CO_2, thereby indicating that these material could be applied as potential adsorbents for storing and capturing CO_2.

Conclusions

We have synthesized a series of inorganic-organic hybrid porous polymers using cubic polyhedral oligomeric silsequioxanes (POSS) and planar halogenated benzene via Heck coupling reaction. The resulting polymers possessed high porosities with S_{BET} of up to 805 m^2 g^{-1} and V_{total} of up to 0.59 cm^3 g^{-1}, and their porosities can be tuned by altering the monomer species and reaction condition. The porosity comparisons of these materials revealed that the surface area, pore volume and microporosity were strongly affected by the monomer species and reaction condition. The factors including long monomer strut length, high monomer reactivity, more connectable sites of monomers, high levels of coupling degrees and the choice of DMF are beneficial to enhance the surface area and pore volume. However, long monomer strut length may also lead to lower surface area and pore volume. DMF might be a positive factor to increase the level of microporosity, whereas increasing connectable sites may afford more mesopores. These results suggest that there is likely no general factor which is optimal for porosity in these polymers and the researchers should comprehensively consider these factors in the preparation of new porous polymers with tunable/ controllable porosity. In addition, these materials could be potentially applied in capturing and storing carbon dioxide.

Acknowledgements

This research was supported by the National Natural Science Foundation of China (21274080 and 21274081), the Key Natural Science Foundation of Shandong Province (ZR2011BZ001), the Fundamental Research Funds of Shandong University and Independent Innovation Foundation of Shandong University.

Notes and references

[a] *National Engineering Research Center for Colloidal Materials, Shandong University, Jinan 250100, P. R. China*
[b] *Key Laboratory of Special Functional Aggregated Materials, Ministry of Education, School of Chemistry and Chemical Engineering, Shandong University, Jinan 250100, P. R. China Fax: +86 531 88564464; Tel: +86 531 88364866; E-mail: fsy@sdu.edu.cn; liuhongzhi@sdu.edu.cn*

† Electronic Supplementary Information (ESI) available: EDS results, BET plots, TGA curves, XRD patterns and FE-SEM images of HPP-1 to HPP-3. See DOI: 10.1039/b000000x/

1 M. E. Davis, *Nature*, 2002, **417**, 813–821.
2 K. Nakanishi and N. Tanaka, *Acc. Chem. Res.*, 2007, **40**, 863–873.
3 H. Furukawa and O. M. Yaghi, *J. Am. Chem. Soc.*, 2009, **131**, 8875–8883.
4 R. J. White, V. Budarin, R. Luque, J. H. Clark and D. J. Macquarriea, *Chem. Soc. Rev.*, 2009, **38**, 3401–3418.
5 M. Yoon, R. Srirambalaji and K. Kim, *Chem. Rev.*, 2012, **112**, 1191–1231.
6 S.-Y. Ding and W. Wang, *Chem. Soc. Rev.*, 2013, **42**, 548–568.
7 Q. Xu, Nanoporous Materials–Synthesis and Applications, CRC Press, Taylor & Francis Group, 2013.
8 V. Valtchev and L. Tosheva, *Chem. Rev.*, 2013, **113**, 6734–6760.
9 D. Wu, F. Xu, B. Sun, R. Fu, H. He and K. Matyjaszewski, *Chem. Rev.*, 2012, **112**, 3959–4015.
10 R. Dawson, A. I. Cooper and D. J. Adams, *Prog. Polym. Sci.*, 2012, **37**, 530–563.
11 A. Thomas, *Angew. Chem. Int. Ed.*, 2010, **49**, 8328–8344.
12 A. I. Cooper, *Adv. Mater.*, 2009, **21**, 1291–1295.
13 N. B. McKeown and P. M. Budd, *Chem. Soc. Rev.*, 2006, **35**, 675–683.
14 J. H. Choi, K. M. Choi, H. J. Jeon, Y. J. Choi, Y. Lee and J. K. Kang, *Macromolecules*, 2010, **43**, 5508–5511.
15 J.-X. Jiang, A. Trewin, D. J. Adams and A. I. Cooper, *Chem. Sci.*, 2011, **2**, 1777–1781.
16 D. Yuan, W. Lu, D. Zhao and H.-C. Zhou, *Adv. Mater.*, 2011, **23**, 3723–3725.
17 M. F. Roll, J. W. Kampf, Y. Kim, E. Yi and R. M. Laine, *J. Am. Chem. Soc.*, 2010, **132**, 10171–10183.
18 J. X. Jiang, F. Su, A. Trewin, C. D. Wood, H. Niu, J. T. A. Jones, Y. Z. Khimyak and A. I. Cooper, *J. Am. Chem. Soc.*, 2008, **130**, 7710–7720.
19 K. V. Rao, S. Mohapatra, C. Kulkarni, T. K. Maji and S. J. George, *J. Mater. Chem.*, 2011, **21**, 12958–12963.
20 K. Zhang, B. Tieke, F. Vilela and P. J. Skabara, *Macro. Rapid Commun.*, 2011, **32**, 825–830.
21 R. M. Laine and M. F. Roll, *Macromolecules*, 2011, **44**, 1073–1109.
22 D. B. Cordes, P. D. Lickiss and F. Rataboul, *Chem. Rev.*, 2010, **110**, 2081–2173.
23 Y. Kim, K. Koh, M. F. Roll, R. M. Laine and A. J. Matzger, *Macromolecules*, 2010, **43**, 6995–7000.
24 W. Chaikittisilp, A. Sugawara, A. Shimojima and T. Okubo, *Chem. Mater.*, 2010, **22**, 4841–4843.
25 D. Wang, L. Xue, L. Li, B. Deng, S. Feng, H. Liu and X. Zhao, *Macro. Rapid Commun.*, 2013, **34**, 861–866.
26 J. J. Morrison, C. J. Love, B. W. Manson, I. J. Shannon and R. E. Morris, *J. Mater. Chem.*, 2002, **12**, 3208–3212.
27 W. Chaikittisilp, A. Sugawara, A. Shimojima and T. Okubo, *Chem. Eur. J.*, 2010, **16**, 6006–6014.
28 D. Wang, W. Yang, L. Li, X. Zhao, S. Feng and H. Liu, *J. Mater. Chem. A*, 2013, **1**, 13549–13558.
29 R. Dawson, A. Laybourn, Y. Z. Khimyak, D. J. Adams and A. I. Cooper, *Macromolecules*, 2010, **43**, 8524–8530.
30 Z. Xie, C. Wang, K. E. deKrafft and W. Lin, *J. Am. Chem. Soc.*, 2011, **133**, 2056–2059.
31 X. Zhu, C. Tian, S. M. Mahurin, S.-H. Chai, C. Wang, S. Brown, G. M. Veith, H. Luo, H. Liu and S. Dai, *J. Am. Chem. Soc.*, 2012, **134**, 10478−10484.
32 P. Kuhn, A. Forget, D. Su, A. Thomas and M. Antonietti, *J. Am. Chem. Soc.*, 2008, **130**, 13333–13337.
33 R. H. Baney, M. Itoh, A. Sakakibara and T. Suzuki, *Chem. Rev.*, 1995, **95**, 1409–1430.
34 J. R. Holst, E. Stöckel, D. J. Adams and A. I. Cooper, *Macromolecules*, 2010, **43**, 8531–8538.
35 T. Ben, H. Ren, S. Ma, D. Cao, J. Lan, X. Jing, W. Wang, J. Xu, F. Deng, J. M. Simmons, S. Qiu and G. Zhu, *Angew. Chem., Int. Ed.*, 2009, **48**, 9457–9460.
36 W. Lu, D. Yuan, D. Zhao, C. I. Schilling, O. Plietzsch, T. Muller, S. Bräse, J. Guenther, J. Blümel, R. Krishna, Z. Li and H.-C. Zhou, *Chem. Mater.*, 2010, **22**, 5964–5972.
37 I. P. Beletskaya and A. V. Cheprakov, *Chem. Rev.*, 2000, **100**, 3009–3066.
38 I. Nischang, O. Brüggemann and I. Teasdale, *Angew. Chem. Int. Ed.*, 2011, **50**, 4592–4596.
39 Y. Peng, T. Ben, J. Xu, M. Xue, X. Jing, F. Deng, S. Qiu and G. Zhu, *Dalton Trans.*, 2011, **40**, 2720–2724.
40 Y. Wu, D. Wang, L. Li, W. Yang, S. Feng and H. Liu, *J. Mater. Chem. A*, 2014, **2**, 2160–2167.
41 A. Fina, D. Tabuani, F. Carniato, A. Frache, E. Boccaleri and G. Camino, *Thermochim. Acta*, 2006, **440**, 36–42.
42 N. Kang, J. H. Park, K. C. Ko, J. Chun, E. Kim, H.-W. Shin, S. M. Lee, H. J. Kim, T. K. Ahn, J. Y. Lee and S. U. Son, *Angew. Chem. Int. Ed.*, 2013, **52**, 6228–6232.
43 K. V. Rao, S. Mohapatra, T. K. Maji and S. J. George, *Chem. Eur. J.*, 2012, **18**, 4505–4509.
44 R. S. Haszeldine, *Science*, 2009, **325**, 1647–1652.

45 N. MacDowell, N. Florin, A. Buchard, J. Hallett, A. Galindo, G. Jackson, C. S. Adjiman, C. K. Williams, N. Shah and P. Fennell, *Energy Environ. Sci.*, 2010, **3**, 1645–1669.
46 S. Choi, J. H. Drese and C. W. Jones, *ChemSusChem*, 2009, 2, 796–854.
47 A. Mallick, S. Saha, P. Pachfule, S. Roy, R. Banerjee, *J. Mater. Chem*., 2010, **20**, 9073–9080.
48 T. Fröschl, U. Hörmann, P. Kubiak, G. Kučrová, M. Pfanzelt, C. K. Weiss, R. J. Behm, N. Hüsing, U. Kaiser, K. Landfester and M. Wohlfahrt-Mehrens, *Chem. Soc. Rev.*, 2012, **41**, 5313–5360.
49 R. Dawson, D. J. Adams and A. I. Cooper, *Chem. Sci.*, 2011, **2**, 1173–1177.
50 R. Dawson, E. Stöckel, J. R. Holst, D. J. Adams and A. I. Cooper, *Energy Environ. Sci.*, 2011, **4**, 4239–4245.